Journal of
Applied and Computational Mechanics

Shahid Chamran
University of Ahvaz

Numerical Simulation of Unsteady Flow toward a Stretching/Shrinking Sheet in Porous Medium Filled with a Hybrid Nanofluid

Saeed Dinarvand[1], Mohammad Yousefi[2], Ali J. Chamkha[3]

[1] Department of Mechanical Engineering, Islamic Azad University, Central Tehran Branch, Tehran, Iran, Email: sae.dinarvand@iauctb.ac.ir

[2] Department of Mechanical Engineering, Islamic Azad University, Central Tehran Branch, Tehran, Iran, Email: myousefi94@yahoo.com

[3] Faculty of Engineering, Kuwait College of Science and Technology, Doha, Kuwait, Email: achamkha@pmu.edu.sa

Abstract. The purpose of this study is to present simulation and numerical solutions to the unsteady flow and heat transfer near stagnation point over a stretching/shrinking sheet in porous medium filled with a hybrid nanofluid. Water (base fluid), nanoparticles of titania and copper were considered as a hybrid nanofluid. It is worth mentioning that evaluating the heat transfer enhancement due to the use of hybrid nanofluids has recently become the center of interest for many researchers. The coupled non-linear boundary-layer equations governing the flow and heat transfer are derived and reduced to a set of coupled non-dimensional equations using the appropriate transformations and then solved numerically as a nonlinear boundary value problem by bvp4c scheme from MATLAB. To validate the modeling of hybrid nanofluid and also numerical procedure, the value of the skin friction and the heat transfer rate for the limited cases of pure water, titania/water and copper/water is obtained and compared with previously reported results that demonstrate an excellent agreement. In the present investigation, the thermal characteristics of hybrid nanofluid are found to be higher in comparison to the base fluid and fluid containing single nanoparticles, respectively. It can be concluded that both skin friction coefficient and local Nusselt number enhance almost linearly with increasing the copper nanoparticle volume fraction (as second nanoparticle). Besides, the porosity and the magnetic effect amplify heat transfer rate, while the unsteadiness parameter has a reducing effect on heat transfer rate in problem conditions.

Keywords: Porous media; Magnetic; Hybrid nanofluid; Two-dimensional stagnation point; Analytic model of hybridity.

1. Introduction

The cooling of electronic devices is one of major industrial requirement nowadays [1,2], but the low thermal conductivity rate of ordinary base fluids including water, ethylene glycol, and oil is a big limitation. To overcome such restrictions, the nanoscale solid particles are submerged into host fluids, which change the thermophysical characteristics of these fluids and enhance the heat transfer rate dramatically [3–9]. The recent developments in nanofluids and their mathematical modeling play a vital role in industrial and nanotechnology [10].

The nanofluids are used in applications such as cooling of electronics, heat exchangers, nuclear reactor safety, hyperthermia, biomedicine, engine cooling, vehicle thermal management, and many others [11–17]. Further, the magneto nanofluids are useful in the manufacturing processes of industries and biomedicine applications [18–22]. Examples include gastric medications, biomaterials for wound treatment, sterilized devices, etc. The magneto nanoparticles can be employed in the elimination of tumors with hyperthermia, targeted drug release, and magnetic resonance imaging.

Different mathematical models have been employed by several authors to describe heat transfer in nanofluids. Among all, the most used ones are those where the concentration of the nanoparticles is constant and the addition of the nanoparticles into the base fluid improved their physical properties [23–26]. Moreover, there are other models that are based on the variation of the physical properties, including thermal dispersion [27] or Brownian motion [28]. A more complex mathematical nanofluid model has been developed by Buongiorno [29] to explore the thermal properties of base fluids. Here, the Brownian motion and thermophoresis are two dominant particle transfer mechanisms in nanofluids. The Brownian motion force tends to uniform nanoparticles in the fluid. The thermophoresis force originates from the temperature gradient in the base fluid. When the size of a particle is very fine (on the order of nanometers), the particle receives more momentum impacts from the fluid molecules on the hot side than that on the cold side; hence, the particle tends to move in a direction opposite to the temperature gradient (the

particle moves from hot to cold). Therefore, there are mass transfer mechanisms in nanofluids because of the Brownian motion and thermophoresis forces. The migrated nanoparticles carry energy and transfer it to the surrounding medium. After that, the researchers investigated the flow of nanofluid under different conditions and different types of nanoparticles. Recently, Celli [30] used Buongiorno's model in combination with a non-homogeneous model to study the free convection flow in a side-heated square cavity filled with a nanofluid. The thermophysical properties of the nanofluid are assumed to be functions of the average volume fraction of nanoparticles dispersed inside the cavity. In 2014, Sheikholeslami et al. [31] have analyzed MHD natural convection of Cu–water nanofluid in a square cavity heated from below and cooled from the side walls. It has been found that the heat transfer rate is an increasing function of heat source length, nanoparticle volume fraction, and Rayleigh number, and a decreasing function of Hartmann number.

In 2015, Mehrez et al. [32] have studied MHD mixed convection flow of Cu–water nanofluid in an open cavity with an isothermal horizontal wall. The authors have shown that an increase in the Hartmann number leads to an attenuation of the recirculation inside the cavity for horizontal and inclined magnetic fields. Also, an inclusion of the nanoparticles leads to an increase in the heat transfer rate and the enhancement rate of heat transfer is higher than the increase rate of entropy generation. A numerical study has been presented by Elshehabey and Ahmed [33] (2015) to investigate the MHD mixed convection of a lid-driven cavity permeated by an inclined uniform magnetic field and filled with nanofluid, using Buongiorno's (2006) nanofluid model. A sinusoidal temperature and nanoparticle volume fraction distributions on both vertical sides is considered, while the horizontal walls are kept adiabatic. In 2018 Aghamajidi et al. [34] investigated the natural-convective flow of an electrically conducting nanofluid adjacent to a spinning down-pointing vertical cone in the presence of transverse magnetic field. Dinarvand et al. [35] have studied the steady axisymmetric mixed convective stagnation-point flow of an incompressible electrically conducting nanofluid over a vertical permeable circular cylinder in the presence of transverse magnetic field. In another study, Dinarvand et al. [36] have studied Tiwari-Das nanofluid scheme to investigate the laminar free-convective flow and heat transfer of an electrically conducting nanofluid in the presence of a transverse magnetic field over a rotating down-pointing vertical cone. Tamim et al. [37] have studied a similarity solution for a steady laminar mixed convection boundary layer flow of a nanofluid near the stagnation point on a vertical permeable plate with a magnetic field and a buoyancy force is obtained by solving a system of nonlinear ordinary differential equations.

Many modern industries deal with heat transfer in some or another way and thus have a strong need for improved heat transfer mediums. This could possibly be nanofluids, because of some potential benefits over normal fluids, large surface area provided by nanoparticles for heat exchange, reduced pumping power due to enhanced heat transfer, minimal clogging, and innovation of miniaturized systems leading to savings of energy and cost. The prediction of heat transfer from irregular surfaces is a topic of fundamental importance for some heat transfer devices (See Misirlioglu et al. [38] , 2005), such as flat plate solar collectors, flat plate condensers in refrigerators, double-wall thermal insulation, underground cable systems, electric machinery, cooling systems of micro-electronic devices, natural circulation in the atmosphere, the molten core of the Earth, etc. In addition, roughened surfaces could be used in the cooling of electrical and nuclear components where the wall heat flux is known. Surfaces are sometimes intentionally roughened to enhance heat transfer, and hence an understanding of natural convection of nanofluids in a porous cavity with wavy walls attains importance. Therefore, the principal aim of the present section is to present a numerical analysis of the natural convection flow in a porous cavity with a wavy bottom and top walls having sinusoidal temperature distributions on vertical walls filled with a nanofluid.

Most of the conducted studies focused on the single type nanoparticle (metallic, metallic oxide or non-metallic) nanofluids. The characteristics of this type of nanofluid are well defined and explored. The advancement in nanomaterial has enabled the production of hybrid nanoparticles (nanocomposites) and recently, there are many researchers investigating on the characteristic of hybrid nanofluids. While each nanofluid generally contains one nanomaterial, hybrid nanofluids contain two dissimilar nanoparticles dispersed in a single component base fluid or a mixture of base fluids [39–41]. It seems that hybrid nanofluids have gained significant attention among the thermal researchers. Hybrid nanofluids can be prepared via two methods: (a) suspending two or more types of nanoparticles into base fluid, (b) suspending composites nanoparticles into base fluid. The objective of inclusion of hybrid nanoparticles in base fluid is to improve heat transfer characteristics of base fluid via combination of nanomaterials' efficient thermo-physical properties [17,42].

In recognition of the benefits of hybrid nanofluids, thermal scientists and researchers have begun to study their synthesis and thermal conductivity characteristics. Abbasi et al. [43] have studied the influence of a functionalization approach on the stability and thermal conductivity of carbon nanotubes (CNTs)/*gamma alumina* (γ-Al$_2$O$_3$) based nanofluids. In their study, they used a solvothermal process to synthesize hybrid nanoparticles and found that the thermal conductivity of the nanofluids seemed to depend on its stability. They concluded that thermal conductivity enhancement up to 14.75% can be achieved at a particle volume fraction of 0.01 for nanofluids with added *gum arabic* (GA) surfactant. In another comprehensive study of hybrid nanofluids, Esfe et al. [44] added *silver* (Ag) and *magnesium oxide* (MgO) (50% each by volume) nanoparticles to water and then evaluate the thermal conductivity of the Ag-MgO/water hybrid nanofluid. They used *cetyl trimethyl ammonium bromide* as surfactant. The authors proposed a new thermal conductivity correlation for the Ag-MgO/water hybrid nanofluid at particle volume fraction ranges between 0 and 2%. They reported good agreement between data predicted by the thermal conductivity correlation and experimental values. Esfe et al. [45] also studied the thermal conductivity of *copper/titanium dioxide* (Cu/TiO$_2$)-water/ethylene glycol hybrid nanofluids. They added Cu and TiO$_2$ nanoparticles to a base fluid and dispersed the nanoparticles via a magnetic stirrer and ultrasonic processor. They then examined the thermal conductivity of the hybrid nanofluid at various particle concentrations (0–2%) and temperatures (30–60 °C). Based on their findings, they developed two new thermal conductivity models using artificial neural network and correlation modeling. The study indicated that both the artificial neural network model and correlation model were able to predict the thermal conductivity of the nanofluid. However, they concluded that the accuracy of the artificial neural network model was higher than that of the correlation model.

In this article, we intend to investigate the unsteady hybrid nanofluid flow and heat transfer near the stagnation point over a stretching/shrinking sheet in porous medium filled with a hybrid nanofluid. Hybrid nanofluid is considered by suspending two different nanoparticles (TiO$_2$ and Cu) in pure water. Based on the similarity transformation, the governing equations with boundary conditions are transformed into a boundary value problem of ordinary differential equations and the Matlab bvp4c ODE solver is effective to solve them. We obtained that the skin friction coefficient and the local Nusselt number increase as both of nanoparticle volume fractions increase. Also the local Nusselt number for three cases of base fluid, nanofluid and hybrid nanofluid has been compared that the highest heat transfer rate is achieved by hybrid nanofluid with highest volume fractions. Moreover, the obtained results depict the impact of various dimensionless parameters such as the permeability parameter (κ), the unsteadiness parameter (ξ), the ratio of stretching/shrinking parameter (ε), the magnetic parameter (M) on velocity, the temperature.
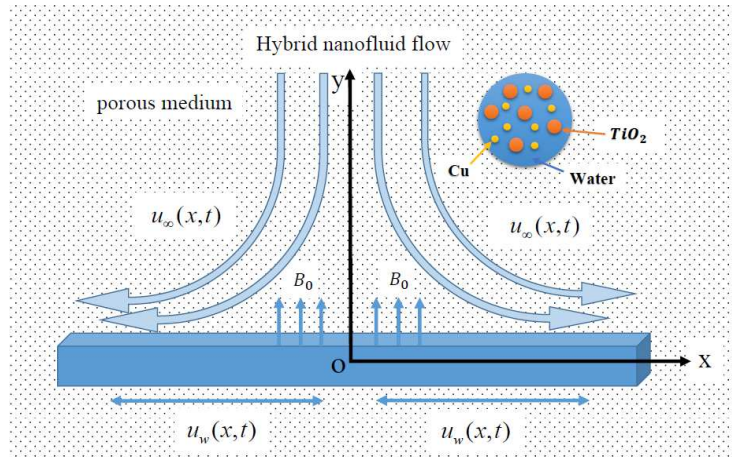
Fig. 1. The schematic of the problem and coordinate system.

2. Hybrid nanofluid flow in porous medium: problem description and mathematical formulation

Consider the two-dimensional laminar stagnation point flow of an electrically conducting Newtonian hybrid nanofluid over a stretching/shrinking sheet in a porous medium as shown in Fig. 1. Cartesian coordinates x and y are taken with the origin O at the stagnation point, and are defined such that the x-axis is measured along the stretching/shrinking sheet and the y-axis is measured normal to it.

It is assumed that the velocity of the inviscid flow is given by $u_\infty = ax/(1-ct)$ and the sheet is stretched with velocity $u_w = bx/(1-ct)$ where a is the strength of the stagnation flow, b is the rate of stretching/shrinking velocity, with $b>0$ for stretching case and $b<0$ for shrinking case and c is a constant. Let the surface temperature T_w be proportional to the distance from the stagnation point, i.e., $T_w(x) = T_\infty + T_0 x$, where T_0 is the characteristic temperature of the hybrid nanofluid. It is assumed that the base fluid (i.e. water) and the nanoparticles are in thermal equilibrium and no slip occurs between them. An important point to note about thermal equilibrium assumption is that, two physical parts (the base fluid and the nanoparticles) are in thermal equilibrium if there is no net flux of thermal energy between them. Besides, when one tells no-slip condition between the base fluid and the nanoparticles, it means that there are no mechanisms that can produce a relative velocity between the nanoparticles and the base fluid. However, this is an assumption for the one-phase model of nanofluid. The basic steady conservation of mass, momentum and energy equations for a nanofluid under a vertical magnetic field through porous media are [47,48]

$$\frac{\partial u}{\partial x} + \frac{\partial v}{\partial y} = 0, \tag{1}$$

$$\frac{\partial u}{\partial t} + u\frac{\partial u}{\partial x} + v\frac{\partial u}{\partial y} = \frac{\partial u_\infty}{\partial t} + u_\infty\frac{\partial u_\infty}{\partial x} + \nu_{hnf}\frac{\partial^2 u}{\partial y^2} + \frac{\nu_{hnf}}{K}(u_\infty - u) + \frac{\sigma B_0^2}{\rho_{hnf}}(u_\infty - u), \tag{2}$$

$$\frac{\partial T}{\partial t} + u\frac{\partial T}{\partial x} + v\frac{\partial T}{\partial y} = \alpha_{hnf}\frac{\partial^2 T}{\partial y^2}, \tag{3}$$

with the initial and boundary conditions [47,48]

$$t < 0: \quad u = v = 0, \quad T = T_\infty \quad \text{for any } x, y. \tag{4}$$

$$t \geq 0: \quad u = u_w(x,t), \quad v = 0, \quad T = T(x) \quad \text{at} \quad y = 0, \\ u \to u_\infty(x,t), \quad T \to T_\infty \quad \text{as} \quad y \to \infty. \tag{5}$$

where, u and v are the velocity components along the x-axes and y-axes, respectively, B_0 is the uniform magnetic field and σ is the electrical conductivity, ν_{hnf} is the kinematic viscosity of the hybrid nanofluid, ρ_{hnf} is the density of the hybrid nanofluid and α_{hnf} is the thermal diffusivity of the hybrid nanofluid, which are given by (see Oztop and Abu-Nada [49]).

In Table 1, ϕ_1 is the solid volume fraction of nanoparticle of Titania (TiO$_2$) and ϕ_2 is the solid volume fraction of the nanoparticle of Copper (Cu), ρ_f is the density of the base fluid and ρ_s is the density of the solid particle. It is worth mentioning that the viscosity of the hybrid nanofluid μ_{hnf} can be approximated as viscosity of a base fluid μ_f containing dilute suspension of fine spherical particles and its expression has been given by Brinkman [50]. In order to obtain the similarity solutions of Eqs.(1)–(3) with the boundary conditions (4) and (5), we introduce the following similarity [24,47,54]:

$$\psi = \left(\frac{a\nu_f}{1-ct}\right)^{1/2} x f(\eta), \qquad \eta = \left(\frac{a}{\nu_f(1-ct)}\right)^{1/2} y, \qquad \theta(\eta) = \frac{T - T_\infty}{T_w - T_\infty}, \tag{6}$$

where, ψ is the stream function defined as $u = \partial\psi / \partial y$ and $v = -\partial\psi / \partial x$, which identically satisfy Eq. (1). Using the non-dimensional variables in (6), Eqs. (2) and (3) reduce to the following ordinary differential equations:

Table 1. Thermophysical properties of TiO₂/water and TiO₂-Cu/water.

Type	Property	The proposed relation
Nanofluid [23,49–52] (TiO₂/water)	Viscosity (μ_{nf})	$\dfrac{\mu_f}{(1-\phi_1)^{2.5}}$
	Density (ρ_{nf})	$(1-\phi_1)\rho_f + \phi_1\rho_{s1}$
	Heat capacity $(\rho C_p)_{nf}$	$(1-\phi_1)(\rho C_p)_f + \phi_1(\rho C_p)_{s1}$
	Thermal conductivity (k_{nf})	$\dfrac{k_{s1}+2k_f-2\phi_1(k_f-k_{s1})}{k_{s1}+2k_f+\phi_1(k_f-k_{s1})}\times(k_f)$
	Diffusivity (α_{nf})	$\dfrac{k_{nf}}{(\rho C_p)_{nf}}$
Hybrid Nanofluid[53] (TiO₂-Cu/water)	Viscosity (μ_{hnf})	$\dfrac{\mu_f}{(1-\phi_1)^{2.5}(1-\phi_2)^{2.5}}$
	Density (ρ_{hnf})	$\left[(1-\phi_2)\{(1-\phi_1)\rho_f+\phi_1\rho_{s1}\}\right]+\phi_2\rho_{s2}$
	Heat capacity $(\rho C_p)_{hnf}$	$\left[(1-\phi_2)\{(1-\phi_1)(\rho C_p)_f+\phi_1(\rho C_p)_{s1}\}\right]+\phi_2(\rho C_p)_{s2}$
	Thermal conductivity (k_{hnf})	$\dfrac{k_{s2}+2k_{nf}-2\phi_2(k_{nf}-k_{s2})}{k_{s2}+2k_{nf}+\phi_2(k_{nf}-k_{s2})}\times\dfrac{k_{s1}+2k_f-2\phi_1(k_f-k_{s1})}{k_{s1}+2k_f+\phi_1(k_f-k_{s1})}\times(k_f)$
	Diffusivity (α_{hnf})	$\dfrac{k_{hnf}}{(\rho C_p)_{hnf}}$

$$f''' + \left\{(1-\phi_1)^{2.5}(1-\phi_2)^{2.5}M + \kappa\right\}(1-f') + (1-\phi_1)^{2.5}(1-\phi_2)^{2.5}\left\{(1-\phi_2)\left[(1-\phi_1)+\phi_1\left(\frac{\rho_{s1}}{\rho_f}\right)\right]+\phi_2\left(\frac{\rho_{s2}}{\rho_f}\right)\right\}\times\left\{ff''+1-f'^2+\xi\left(1-f'-\frac{1}{2}\eta f''\right)\right\}=0, \tag{7}$$

$$\frac{k_{hnf}}{k_f}\theta'' + Pr\left\{(1-\phi_2)\left[(1-\phi_1)+\phi_1\left(\frac{(\rho C_p)_{s1}}{(\rho C_p)_f}\right)\right]+\phi_2\left(\frac{(\rho C_p)_{s2}}{(\rho C_p)_f}\right)\right\}\times\left\{f\theta'-f'\theta-\frac{\xi}{2}\eta\theta'\right\}=0, \tag{8}$$

where κ is the permeability parameter of the media, $\xi = c/a$ is unsteadiness parameter, with $\xi > 0$ for accelerating flow, $\xi < 0$ for decelerating flow and $\xi = 0$ for steady state flow. $Pr = \nu_f/\alpha_f$ is the Prandtl number of the base fluid and primes denote differentiation with respect to η. The boundary conditions (4) become

$$f(0)=0,\ f'(0)=b/a=\varepsilon,\ \ \theta(0)=1,\ \ f'(\eta)\to 1,\ \theta(\eta)\to 0\ \text{ as }\ \eta\to\infty \tag{9}$$

The velocity ratio parameter ε is defined as the ratio of stretching rate of the sheet and strength of the free stream. $\varepsilon > 0$, $\varepsilon < 0$ and $\varepsilon = 1$ correspond to stretching, shrinking sheets and the flow with no boundary layer ($u_w = u_\infty$), respectively, while $\varepsilon = 0$ is the planar stagnation flow towards a stationary sheet. The skin friction coefficient C_f and the local Nusselt number Nu_x are the physical quantities of interest which are defined as

$$C_f = \frac{\tau_w}{\rho_f u_\infty^2}, \qquad Nu_x = \frac{xq_w}{k_f(T_w-T_\infty)}, \tag{10}$$

where τ_w is the surface shear stress and q_w is the surface heat flux which are given by

$$\tau_w = \mu_{hnf}\left(\frac{\partial u}{\partial y}\right)_{y=0}, \qquad q_w = -k_{hnf}\left(\frac{\partial T}{\partial y}\right)_{y=0}. \tag{11}$$

Substituting (6) into Eqs. (10) and (11), we obtain

$$C_f(Re_x)^{1/2} = \frac{1}{(1-\phi_1)^{2.5}(1-\phi_2)^{2.5}}f''(0), \qquad Nu_x(Re_x)^{-1/2} = -\frac{k_{hnf}}{k_f}\theta'(0). \tag{12}$$

where $Re_x = u_\infty x/\nu_f$ is the local Reynolds number.

3. Validation of numerical procedure, results and discussion

The system of nonlinear ordinary differential equations (7) and (8) with the boundary conditions (9) are solved numerically using the bvp4c scheme from MATLAB and the results are reported for some values of the permeability parameter (κ), the unsteadiness parameter (ξ), the ratio of stretching/shrinking parameter (ε), the magnetic parameter (M) on the velocity, the temperature, the skin friction parameter and the local Nusselt number. Moreover, the effect of solid volume fraction of copper (ϕ_2) on the skin friction parameter and the local Nusselt number is investigated. Solutions to the given problem are presented in the graphical and tabular forms.

In Table 2, we can see the physical properties of the base fluid and the nanoparticles at 25°C. Moreover, in the present study, it is assumed that the nanoparticles are in thermal equilibrium and no slip occurs between them. In order to verify the accuracy of the numerical results, the validity of the developed numerical code has been checked for limiting cases as follows. In the first case, we consider steady-state flow of a regular fluid ($\phi_1 = \phi_2 = 0$) through nonporous medium ($\kappa = 0$) and in the absence of magnetic field ($M = 0$). Then we compare our results with those given by Suali et al. [55], Wang [56] and Khalili et al. [54] for different values of velocity ratio ε (Table 3). In the next step, we compare our results with those given by Bachok et al. [57] and Khalili et al. [54] for some values of ξ, the different nanoparticles and constant wall temperature, when $\varepsilon = \kappa = M = 0$ (Table 4). The comparisons are found to be in excellent agreement, and thus give confidence that numerical results obtained are accurate.

Table 2. Thermophysical properties of the base fluid and the nanoparticles (See[58,59]).

Physical properties	Base fluid (water)	TiO$_2$	Cu
$C_P\,(J\,/\,kg\,K)$	4179	686.2	385
$\rho\,\,(kg\,/\,m^3)$	997.1	4250	8933
$k\,(W\,/\,mK)$	0.613	8.954	400
$\alpha \times 10^7\,(m^2/s)$	1.47	30.7	1163.1
Nanoparticles size(nm)	--	50	20

Table 3. The variation of $f''(0)$ with some values of ε, for the steady state flow of a regular fluid $(\phi_1 = \phi_2 = 0)$, when $\xi = \kappa = M = 0$ and Pr=6.2.

ε	Wang[56]	Suali et al.[55]	Khalili et al.[54]	Present study
3	-	-4.276545	-4.276541	-4.276541
0.2	1.05113	1.051130	1.051130	1.051130
0.1	1.14656	1.146561	1.146561	1.146561
-0.1	1.30860	1.308602	1.308602	1.308602
-1	1.32882	1.328817	1.328817	1.328817
-1.15	1.08223	1.082232	1.082231	1.082231

Table 4. The variation of $f''(0)$ and $-\theta'(0)$ with some values of ξ, for the steady state flow of *titania/water* $(\phi_1 = 0.1, \phi_2 = 0)$ and *copper-water* $(\phi_1 = 0, \phi_2 = 0.1)$ on stationary sheet with constant wall temperature, when $\varepsilon = \kappa = M = 0$.

ξ		Bachok et al. [57]		Khalili et al. [54]		Present study	
		Cu	TiO$_2$	Cu	TiO$_2$	Cu	TiO$_2$
1	$f''(0)$	1.7604	1.5128	1.760398	1.512796	1.760399	1.512799
	$-\theta'(0)$	0.4681	0.4076	0.468134	0.407566	0.468238	0.407425
-1	$f''(0)$	1.0845	0.9320	1.084530	0.931990	1.084530	0.931990
	$-\theta'(0)$	1.4957	1.4910	1.495740	1.490996	1.495421	1.490697
-2	$f''(0)$	0.6499	0.5585	0.649877	0.558471	0.649878	0.558492
	$-\theta'(0)$	1.8532	1.8651	1.853218	1.865106	1.853308	1.865036
-3	$f''(0)$	0.1045	0.0898	-	-	0.104471	0.089775
	$-\theta'(0)$	2.1550	2.1801	-	-	2.226761	2.238459
-4	$f''(0)$	-0.6757	-0.5806	-	-	-0.675674	-0.580642
	$-\theta'(0)$	2.4089	2.4461	-	-	2.398322	2.427920

Table 5. The skin friction coefficient and local Nusselt number for different values of *titania* volume fraction (ϕ_1) and *copper* volume fraction (ϕ_2) on stationary sheet with constant wall temperature, when $\varepsilon = 0.2$, $\xi = \kappa = M = 1$ and Pr=6.2.

ϕ_1	ϕ_2	$(\mathrm{Re}_x)^{1/2}C_f = \dfrac{1}{(1-\phi_1)^{2.5}(1-\phi_2)^{2.5}}f''(0)$	$(\mathrm{Re}_x)^{-1/2}Nu_x = -\dfrac{k_{hnf}}{k_f}\theta'(0)$
0	0	1.69816	1.71374
0.05	0	1.9046	1.82809
0.1	0	2.14995	1.94679
0	0.05	2.01145	1.88594
0	0.1	2.36227	2.06198
0.05	0.05	2.24546	2.01157
0.1	0.05	2.51163	2.13751
0.1	0.1	2.90971	2.32972

3.1. Velocity and temperature analysis of titania-copper/water hybrid nanofluid flow

In this section, the results are shown and compared with both regular Newtonian fluid (water) and single-particle nanofluid (TiO$_2$/water) cases to study the boundary layers behavior of the two-dimensional stagnation point flow of TiO$_2$-Cu/water hybrid nanofluid. For the present investigation, we assume that the value of Prandtl number Pr is equal with 6.2 (for water). In addition, the value of the cumulative nanoparticle volume fraction f_c in considered to vary from 0 (regular Newtonian fluid, when $\phi_1 = \phi_2 = 0$) to 0.1 (hybrid nanofluid, when $\phi_1 = 0.1, \phi_2 = 0.1$) as pointed out by Oztop and Abu-Nada for single-particle nanofluid [49]. Fig. 2 depicts the dimensionless velocity and temperature profiles for regular fluid $(\phi_1 = \phi_2 = 0)$, nanofluid $(\phi_1 = 0.1, \phi_2 = 0)$ and hybrid nanofluid $(\phi_1 = 0.1, \phi_2 = 0.1)$. From Fig. 2, it is observed that the highest value of $f'(\eta)$ is related to hybrid nanofluid and the lowest one belongs to regular fluid. The comparison of dimensionless velocity and temperature profiles for nanofluid $(\phi_1 = 0.1, \phi_2 = 0)$ and hybrid nanofluids $(\phi_1 = 0.1, \phi_2 = 0.05, 0.1)$ is illustrated in Fig. 3. We can obviously see that hybrid nanofluid with greater nanoparticle volume fraction of Copper (ϕ_2) has highest velocity profiles in comparison to others. The dimensionless velocity and temperature profiles for hybrid nanofluid with various values of the velocity ratio parameter (ε) is shown in Fig. 4. The lowest temperature occurs when the velocity ratio parameter (ε) is highest and the highest one is related to ε = -0.5. This is due to the hybridity boosts the temperature distribution in the boundary layer. Fig. 5 determines the effect of magnetic parameter on dimensionless velocity and temperature profiles, for fixed values of nanoparticle volume fractions $(\phi_1 = 0.1, \phi_2 = 0.1)$. A drag-like force that called Lorentz force is created by the infliction of the vertical magnetic field to the electrically conducting fluid. This force has the tendency to slow down the flow over the surface. According to this explanation, the hydrodynamic boundary layer thickness gets depressed and also the temperature distribution decreases slightly with the increase in the magnetic parameter.

Fig. 6 illustrates the influence of the unsteadiness parameter (ξ) on dimensionless velocity and temperature profiles for hybrid nanofluid $(\phi_1 = 0.1, \phi_2 = 0.1)$. This figure is plotted for steady state case $(\xi = 0)$ and accelerating flow $(\xi > 0)$. It is clearly observable that the highest unsteadiness parameter (ξ) has greater velocity profile.
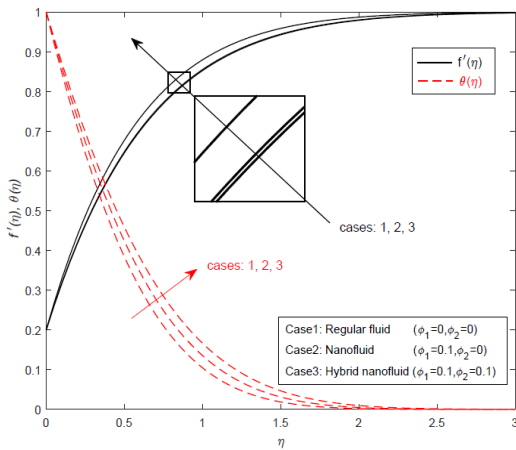
Fig. 2. Dimensionless velocity and temperature profiles for the regular fluid, the nanofluid and the hybrid nanofluid, when $\varepsilon = 0.2$, $\xi = 1$, $\kappa = M = 0$ and Pr=6.2.
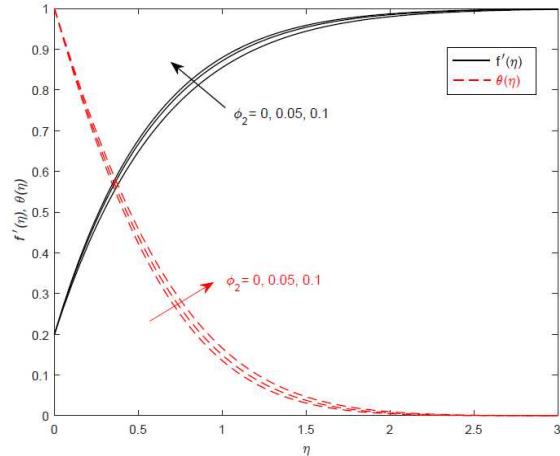

Fig. 3. Dimensionless velocity and temperature profiles for the various values of ϕ_2, when $\varepsilon = 0.2$, $\xi = 1$, $\kappa = M = 0$, $\phi_1 = 0.1$ and Pr=6.2.
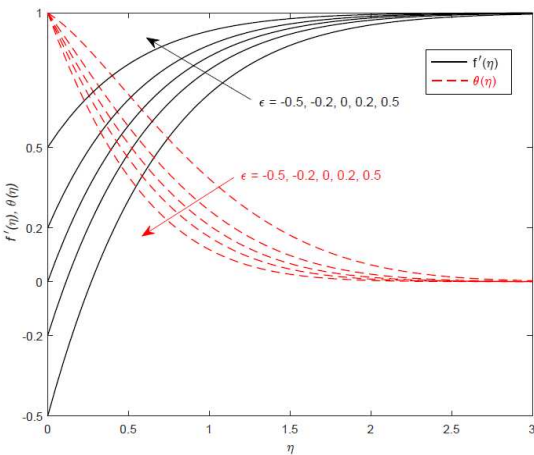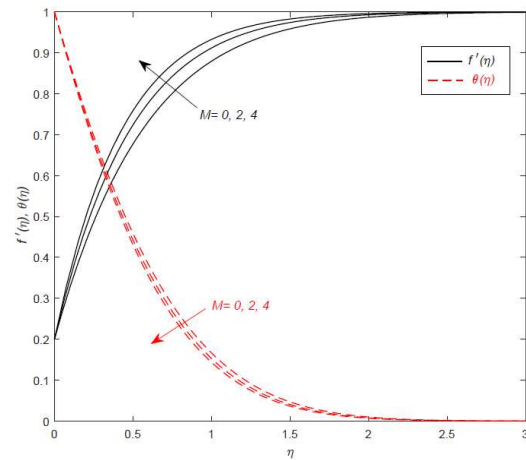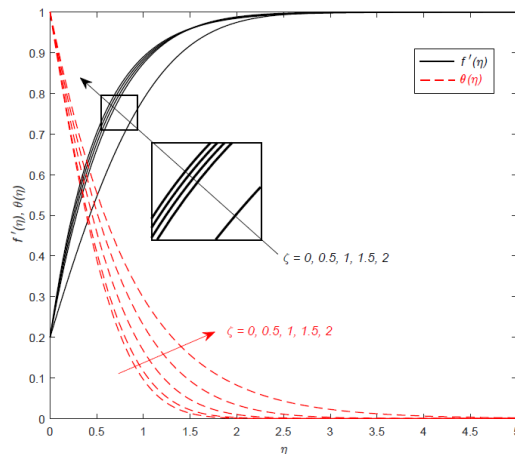

Fig. 4. Dimensionless velocity and temperature profiles for the various values of ε, when $\xi = 1$, $\kappa = M = 0$, $\phi_1 = \phi_2 = 0.1$ and Pr=6.2.

Fig. 5. Dimensionless velocity and temperature profiles for the various values of M, when $\varepsilon = 0.2$, $\xi = 1$, $\kappa = 0$, $\phi_1 = \phi_2 = 0.1$ and Pr=6.2.

Fig. 6. Dimensionless velocity and temperature profiles for the various values of ξ, when $\varepsilon = 0.2$, $\kappa = M = 0$, $\phi_1 = \phi_2 = 0.1$ and Pr=6.2.

3.2. Effect of emerging parameters on skin friction and heat transfer

In Fig. 7, the dimensionless skin friction coefficients $Re_x^{1/2}C_{fx}$ and the local Nusselt number $Re_x^{-1/2}Nu_x$ versus *copper* nanoparticle volume fraction (ϕ_2) has been plotted for a fixed value of *titania* nanoparticle volume fraction ($\phi_1 = 0.1$) and various values of magnetic parameter (M). It can be seen that both skin friction coefficient and local Nusselt number enhance almost linearly with increasing the *copper* nanoparticle volume fraction (ϕ_2) for all magnetic parameter values. From this figure, the skin friction coefficient $Re_x^{1/2}C_{fx}$ and the local Nusselt number enhance by increasing values of magnetic parameter (M). Fig. 8 shows the dimensionless skin friction coefficient $Re_x^{1/2}C_{fx}$ and the local Nusselt number $Re_x^{-1/2}Nu_x$ versus copper nanoparticle volume fraction (ϕ_2) for a fixed value of *titania* nanoparticle volume fraction ($\phi_1 = 0.1$) and various values of permeability parameter (κ). It is observed that both skin friction coefficient and local Nusselt number increase almost linearly with increasing
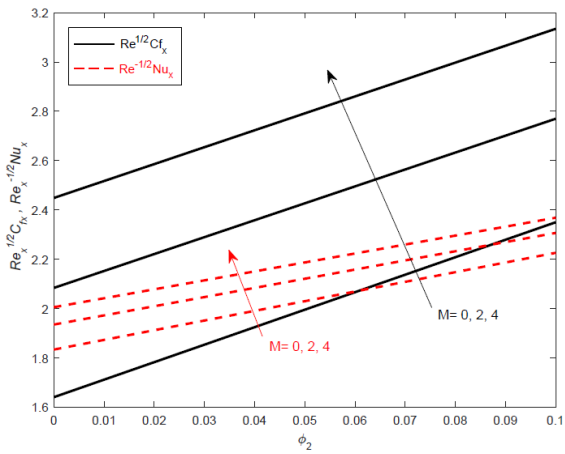
Fig. 7. The effect of magnetic parameter M on the dimensionless skin friction coefficient $\mathrm{Re}_x^{1/2}\, C_{fx}$ and the local Nusselt number $\mathrm{Re}_x^{-1/2}\, Nu_x$ versus copper nanoparticle volume fraction ϕ_2, when $\phi_1 = 0.1, \xi = 1, \varepsilon = 0.2, \kappa = 0$ and $Pr = 6.2$.
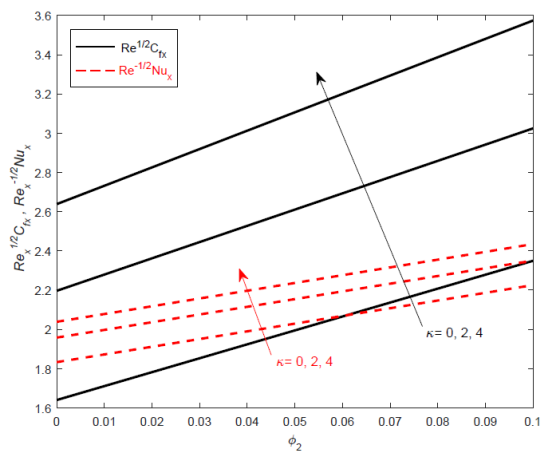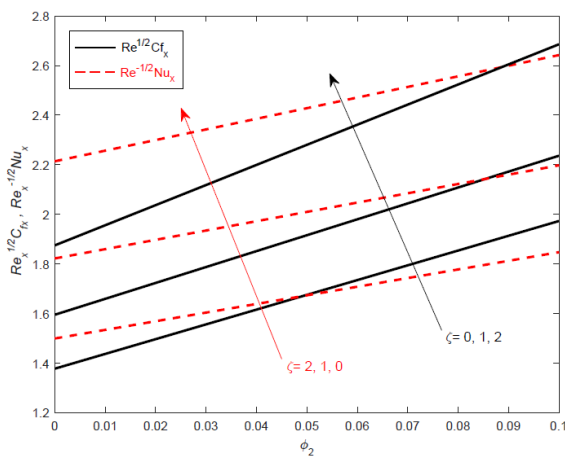

Fig. 8. The effect of permeability parameter κ on the dimensionless skin friction coefficient $\mathrm{Re}_x^{1/2}\, C_{fx}$ and the local Nusselt number $\mathrm{Re}_x^{-1/2}\, Nu_x$ versus copper nanoparticle volume fraction ϕ_2, when $\phi_1 = 0.1, \xi = 1, \varepsilon = 0.2, M = 0$ and $Pr = 6.2$.

Fig. 9. The effect of unsteadiness parameter ξ on the dimensionless skin friction coefficient $\mathrm{Re}_x^{1/2}\, C_{fx}$ and the local Nusselt number $\mathrm{Re}_x^{-1/2}\, Nu_x$ versus copper nanoparticle volume fraction ϕ_2, when $\phi_1 = 0.1, \varepsilon = 0.2, \kappa = M = 0$ and $Pr = 6.2$.
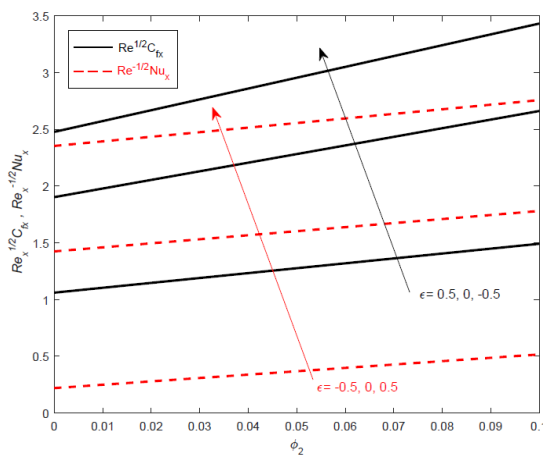

Fig. 10. The effect of velocity ratio parameter ε on the dimensionless skin friction coefficient $\mathrm{Re}_x^{1/2}\, C_{fx}$ and the local Nusselt number $\mathrm{Re}_x^{-1/2}\, Nu_x$ versus copper nanoparticle volume fraction ϕ_2, when $\phi_1 = 0.1, \xi = 1, \kappa = M = 0$ and $Pr = 6.2$ and variation values of $\varepsilon = 0.2$.

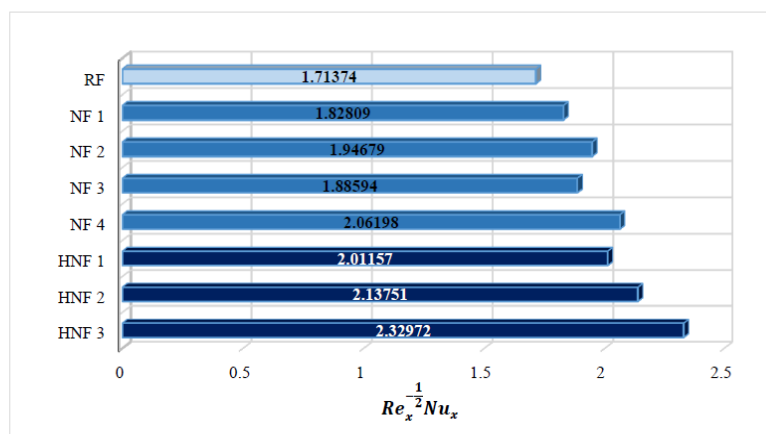| Type	φ_{TiO_2}	φ_{Cu}
Regular fluid	0	0
Nanofluid 1	0.05	0
Nanofluid 2	0.1	0
Nanofluid 3	0	0.05
Nanofluid 4	0	0.1
Hybrid nanofluid 1	0.05	0.05
Hybrid nanofluid 2	0.1	0.05
Hybrid nanofluid 3	0.1	0.1

Fig. 11. The local Nusselt number $\mathrm{Re}_x^{-1/2}\, Nu_x$ for various cases of regular fluid, nanofluid and hybrid nanofluid according to the enclosed list, when $\xi = \kappa = M = 1, \varepsilon = 0.2$ and $Pr = 6.2$.

the *copper* nanoparticle volume fraction (ϕ_2) for all permeability parameter (κ) values. From this figure, the skin friction coefficient $\mathrm{Re}_x^{1/2} C_{fx}$ and the local Nusselt number enhance by increasing values of permeability parameter. In Fig. 9, the dimensionless skin friction coefficient $\mathrm{Re}_x^{1/2} C_{fx}$ and the local Nusselt number $\mathrm{Re}_x^{-1/2} Nu_x$ versus copper nanoparticle volume fraction (ϕ_2) have been plotted for a fixed value of *titania* nanoparticle volume fraction ($\phi_1 = 0.1$) and various values of unsteadiness parameter (ξ). It can be observed clearly that both skin friction coefficient and local Nusselt number increase almost linearly as the copper nanoparticle volume fraction (ϕ_2) increases. This figure, shows clearly that the skin friction coefficient

$Re_x^{1/2}C_{fx}$ grows by increasing values of unsteadiness parameter (ξ), while, the local Nusselt number decrease by increasing values of unsteadiness parameter (ξ). The dimensionless skin friction coefficient $Re_x^{1/2}C_{fx}$ and the local Nusselt number $Re_x^{-1/2}Nu_x$ versus *copper* nanoparticle volume fraction (ϕ_2) is depicted in Fig. 10. This figure has been plotted for a fixed value of *titania* nanoparticle volume fraction ($\phi_1 = 0.1$) and various values of velocity ratio parameter (ε). These results clarify that both skin friction coefficient and local Nusselt number enhance almost linearly with increasing the *copper* nanoparticle volume fraction (ϕ_2) for all velocity ratio parameter values. This figure, shows obviously that the skin friction coefficient $Re_x^{1/2}C_{fx}$ enhance by decreasing values of velocity ratio parameter (ε), while, the local Nusselt number decrease by increasing values of unsteadiness parameter (ξ). Fig. 11 compares the local Nusselt number for eight cases and three types of fluids (regular fluid, nanofluid and hybrid nanofluid). It is observed that the local Nusselt number of hybrid nanofluid is greater than the regular fluid and single nanoparticle nanofluid. In fact, the local heat transfer rate boosts with enhancing first and second nanoparticle masses for all cases. As we know, when the mass of the nanoparticles enhances, the effective thermal conductivity increases and affects the heat transfer rate of the working fluid. Therefore, we can clearly see that employing hybrid nanofluid enhance the heat transfer rate and is more effective than single nanoparticle nanofluid. Table 5 illustrates some values of skin friction coefficient and local Nusselt number in the steady state flow for different values of titania volume fraction and copper volume fraction on stationary sheet with constant wall temperature. It is obviously can determine that increasing the volume fraction of both nanoparticles increases the skin friction coefficient and the local Nusselt number and the greatest values of them are for hybrid nanofluid.

4. Conclusion

In this article, the unsteady flow and heat transfer near stagnation point over a stretching/shrinking sheet in porous medium filled with a hybrid nanofluid has been investigated. Hybrid nanofluid is considered by suspending two different nanoparticles (TiO$_2$ and Cu) in pure water. Based on the similarity transformation, the governing equations with the relevant boundary conditions are transformed into a boundary value problem of ordinary differential equations. Matlab *bvp4c* ODE solver was effective to solve the system of ODE. Moreover, the obtained results depict the impact of various dimensionless parameters such as the permeability parameter (κ), the unsteadiness parameter (ξ), the ratio of stretching/shrinking parameter (ε), the magnetic parameter (M) on the velocity, the temperature, the skin friction coefficient and the local Nusselt number. Main findings are listed below:

- Our computation demonstrates that skin friction coefficient and the local Nusselt number increase as *copper* volume fraction (ϕ_2) increases.

- The highest skin friction and heat transfer rate are achieved for hybrid nanofluid (TiO$_2$-Cu/water).

- Hybridity boost the heat transfer enhancement.

- Hybrid nanofluid is more efficient compared to nanofluid.

- Increasing the magnetic parameter, improves the heat transfer and the skin friction.

Author Contributions

S.D. wrote the discussions and the interpretation of the results and co-wrote the manuscript. M.Y. and A.J.C. proposed the mathematical and the numerical models and conducted the numerical analysis. All authors originated the developed problem and reviewed the manuscript.

Acknowledgments

Conflict of Interest

The authors declared no potential conflicts of interest with respect to the research, authorship and publication of this article.

Funding

Data Availability Statements

The datasets generated and/or analyzed during the current study are available from the corresponding author on reasonable request.

Nomenclature

T$_0$	the strength of the stagnation flow		*Greek symbols*	
b	the rate of stretching/shrinking velocity		α	thermal diffusivity [m^2/s]
c	constant		ϕ	nanoparticle volume fraction
B$_0$	uniform magnetic field [N]		η	similarity variable
σ	electrical conductivity [S/m]		$\theta(\eta)$	dimensionless temperature
C$_f$	skin friction coefficient		μ	dynamic viscosity [Kg/ms]
C$_p$	specific heat capacity [J/Kg.K]		ν	kinematic viscosity [m^2/s]
g	acceleration due to gravity [m/s^2]		ρ	fluid density [Kg/m^3]
k	thermal conductivity [W/mK]		τ_w	wall shear stress [Kg/ ms^2]
Nu$_x$	local Nusselt number		*Subscripts*	
Re$_x$	local Reynolds number		w	condition at the surface of the plate

Pr	Prandtl number	∞	ambient condition
q_w	surface heat flux [W/m²]	f	fluid
T	fluid temperature [K]	nf	nanofluid
T_w	surface temperature [K]	hnf	hybrid nanofluid
T_∞	ambient temperature [K]	1	*titania* nanoparticle
u, v	velocity components [m/s]	2	*copper* nanoparticle
x, y	Cartesian coordinates [m]	s_1	first nanoparticle (TiO₂)
$f(\eta)$	the first component of velocity profile	s_2	second nanoparticle (Cu)
$g(\eta)$	the second component of velocity profile	$'$	differentiation with respect to η

References

[1] Kuznetsov GV, Sheremet MA. New approach to the mathematical modeling of thermal regimes for electronic equipment. *Russ Microelectron.* 37(2), 2008, 131–8.

[2] Kuznetsov GV, Sheremet MA. On the possibility of controlling thermal conditions of a typical element of electronic equipment with a local heat source via natural convection. *Russ Microelectron.* 39(6), 2010, 427–42.

[3] Choi SUS, Eastman JA. Enhancing thermal conductivity of fluids with nanoparticles, *The Proceeding of the 1995 ASME International Mechanical Engineering Congress and Exposition*, San Francisco, USA, ASME, FED 231/MD. 66, 1995, 99–105.

[4] Ding Y, Chen H, Wang L, Yang C-Y, He Y, Yang W, et al. Heat transfer intensification using nanofluids. *KONA Powder Part J.* 25, 2007, 23–38.

[5] Dinarvand S. Nodal/saddle stagnation-point boundary layer flow of CuO–Ag/water hybrid nanofluid: a novel hybridity model. *Microsyst Technol.* 25, 2019, 2609-2623.

[6] Usman M, Soomro FA, Haq RU, Wang W, Defterli O. Thermal and velocity slip effects on Casson nanofluid flow over an inclined permeable stretching cylinder via collocation method. *Int J Heat Mass Transf.* 122, 2018, 1255–63.

[7] Usman M, Haq RU, Hamid M, Wang W. Least square study of heat transfer of water based Cu and Ag nanoparticles along a converging/diverging channel. *J Mol Liq.* 249, 2018, 856–67.

[8] Usman M, Hamid M, Haq RU, Wang W. Heat and fluid flow of water and ethylene-glycol based Cu-nanoparticles between two parallel squeezing porous disks: LSGM approach. *Int J Heat Mass Transf.* 123, 2018, 888–95.

[9] Hamid M, Usman M, Zubair T, Haq RU, Wang W. Shape effects of MoS 2 nanoparticles on rotating flow of nanofluid along a stretching surface with variable thermal conductivity: A Galerkin approach. *Int J Heat Mass Transf.* 124, 2018, 706–14.

[10] Shenoy A, Sheremet M, Pop I. *Convective flow and heat transfer from wavy surfaces: viscous fluids, porous media, and nanofluids.* CRC Press; 2016.

[11] Das SK, Choi SU, Yu W, Pradeep T. *Nanofluids: science and technology.* John Wiley & Sons; , 2007.

[12] Schaefer H-E. *Nanoscience: the science of the small in physics, engineering, chemistry, biology and medicine.* Springer Science & Business Media; 2010.

[13] Rao Y. Nanofluids: stability, phase diagram, rheology and applications. *Particuology.* 8(6), 2010, 549–55.

[14] Dinarvand S, Rostami MN. An innovative mass-based model of aqueous zinc oxide–gold hybrid nanofluid for von Kármán's swirling flow. *J Therm Anal Calorim.* (2019) 1–11.

[15] Kleinstreuer C. *Microfluidics and nanofluidics: theory and selected applications.* John Wiley & Sons; , 2013.

[16] Yousefi M, Dinarvand S, Eftekhari Yazdi M, Pop I. Stagnation-point flow of an aqueous titania-copper hybrid nanofluid toward a wavy cylinder. *Int J Numer Methods Heat Fluid Flow.* 28(7), 2018, 1716–35.

[17] Sarkar J, Ghosh P, Adil A. A review on hybrid nanofluids: recent research, development and applications. *Renew Sustain Energy Rev.* 43, 2015, 164–77.

[18] Brust M, Walker M, Bethell D, Schiffrin DJ, Whyman R. Synthesis of thiol-derivatised gold nanoparticles in a two-phase liquid–liquid system. *J Chem Soc Chem Commun.* 7, 1994, 801–2.

[19] Chengara A, Nikolov AD, Wasan DT, Trokhymchuk A, Henderson D. Spreading of nanofluids driven by the structural disjoining pressure gradient. *J Colloid Interface Sci.* 280(1), 2004, 192–201.

[20] C.K Chen, Cho CC. Electrokinetically-driven flow mixing in microchannels with wavy surface. *J Colloid Interface Sci.* 312(2), 2007, 470–80.

[21] Rostami MN, Dinarvand S, Pop I. Dual solutions for mixed convective stagnation-point flow of an aqueous silica–alumina hybrid nanofluid. *Chinese J Phys.* 56(5), 2018, 2465–78.

[22] Bahiraei M, Materials MH-J of M and M, 2015 U. Flow and heat transfer characteristics of magnetic nanofluids: a review. *J Magn Magn Mater.* 374, 2015, 125–38.

[23] Khanafer K, Vafai K, Lightstone M. Buoyancy-driven heat transfer enhancement in a two-dimensional enclosure utilizing nanofluids. *Int J Heat Mass Transf.* 46, 2003, 3639–53.

[24] Tiwari RK, Das MK. Heat transfer augmentation in a two-sided lid-driven differentially heated square cavity utilizing nanofluids. *Int J Heat Mass Transf.* 50(9–10), 2007, 2002–18.

[25] Bondareva NS, Sheremet MA, Pop I. Magnetic field effect on the unsteady natural convection in a right-angle trapezoidal cavity filled with a nanofluid: Buongiorno's mathematical model. *Int J Numer Methods Heat Fluid Flow.* 25(8), 2015, 1924–46.

[26] Haq RU, Soomro FA, Mekkaoui T, Al-Mdallal QM. MHD natural convection flow enclosure in a corrugated cavity filled with a porous medium. *Int J Heat Mass Transf.* 121, 2018, 1168–78.

[27] Grosan T, Pop I. Forced convection boundary layer flow past nonisothermal thin needles in nanofluids. *J Heat Transfer.* 133, 2011, 054503.

[28] Kleinstreuer C, Li J, Koo J. Microfluidics of nano-drug delivery. *Int J Heat Mass Transf.* 51(23–24), 2008, 5590–7.

[29] Buongiorno J. Convective transport in nanofluids. *J Heat Transfer.* 128(3), 2006, 240–50.

[30] Celli M. Non-homogeneous model for a side heated square cavity filled with a nanofluid. *Int J Heat Fluid Flow.* 44, 2013, 327–35.

[31] Sheikholeslami M, Bandpy MG, Ellahi R, Zeeshan A. Simulation of MHD CuO–water nanofluid flow and convective heat transfer considering Lorentz forces. *J Magn Magn Mater.* 369, 2014, 69–80.

[32] Mehrez Z, El Cafsi A, Belghith A, Le Quéré P. MHD effects on heat transfer and entropy generation of nanofluid flow in an open cavity. *J Magn Magn Mater.* 374, 2015, 214–24.

[33] Elshehabey HM, Ahmed SE. MHD mixed convection in a lid-driven cavity filled by a nanofluid with sinusoidal temperature distribution on the both vertical walls using Buongiorno's nanofluid model. *Int J Heat Mass Transf.* 88, 2015, 181–202.

[34] Aghamajidi M, Yazdi M, Dinarvand S, Pop I. Tiwari-Das nanofluid model for magnetohydrodynamics (MHD) natural-convective flow of a nanofluid adjacent to a spinning down-pointing vertical cone. *Propuls Power Res.* 7(1), 2018, 78–90.

[35] Dinarvand S, Hosseini R, Pop I. Axisymmetric mixed convective stagnation-point flow of a nanofluid over a vertical permeable cylinder by Tiwari-Das nanofluid model. *Powder Technol.* 311, 2017, 147–56.

[36] Dinarvand S, Pop I. Free-convective flow of copper/water nanofluid about a rotating down-pointing cone using Tiwari-Das nanofluid scheme. *Adv Powder Technol.* 28(3), 2017, 900–9.

[37] Tamim H, Dinarvand S, Hosseini R, Rahimi H, Pop I. Steady laminar mixed convection stagnation-point flow of a nanofluid over a vertical permeable surface in the presence of a magnetic field. *J Appl Mech Tech Phys.* 57(6), 2016 Nov 9, 1031–41.

[38] Misirlioglu A, Baytas AC, Pop I. Free convection in a wavy cavity filled with a porous medium. *Int J Heat Mass Transf.* 48(9), 2005, 1840–50.

[39] Esfe MH, Yan W-M, Akbari M, Karimipour A, Hassani M. Experimental study on thermal conductivity of DWCNT-ZnO/water-EG nanofluids. *Int Commun Heat Mass Transf.* 68, 2015, 248–51.

[40] Babu JAR, Kumar KK, Rao SS. State-of-art review on hybrid nanofluids. *Renew Sustain Energy Rev.* 77, 2017, 551–65.

[41] Esfe MH, Afrand M, Yan W-M, Yarmand H, Toghraie D, Dahari M. Effects of temperature and concentration on rheological behavior of MWCNTs/SiO2 (20–80)-SAE40 hybrid nano-lubricant. *Int Commun Heat Mass Transf.* 76, 2016, 133–8.

[42] Usman M, Hamid M, Zubair T, Haq RU, Wang W. Cu-Al2O3/Water hybrid nanofluid through a permeable surface in the presence of nonlinear radiation and variable thermal conductivity via LSM. *Int J Heat Mass Transf.* 126, 2018, 1347–56.

[43] Abbasi SM, Rashidi A, Nemati A, Arzani K. The effect of functionalisation method on the stability and the thermal conductivity of nanofluid hybrids of carbon nanotubes/gamma alumina. *Ceram Int.* 39(4), 2013, 3885–91.

[44] Esfe MH, Arani AAA, Rezaie M, Yan W-M, Karimipour A. Experimental determination of thermal conductivity and dynamic viscosity of Ag–MgO/water hybrid nanofluid. *Int Commun Heat Mass Transf.* 66, 2015, 189–95.

[45] Esfe MH, Wongwises S, Naderi A, Asadi A, Safaei MR, Rostamian H, et al. Thermal conductivity of Cu/TiO2–water/EG hybrid nanofluid: experimental data and modeling using artificial neural network and correlation. *Int Commun Heat Mass Transf.* 66, 2015, 100–4.

[46] STOKES GG. *Mathematical and physical papers.* Cambridge Cambridge Univ Press. 1, 1880.

[47] Hiemenz K. Die Grenzschicht an einem in den gleichformigen Flussigkeitsstrom eingetauchten geraden Kreiszylinder. *Dingler's Ploytech.* 321, 1911, 326.

[48] Tiwari RK, Das MK. Heat transfer augmentation in a two-sided lid-driven differentially heated square cavity utilizing nanofluids. *Int J Heat Mass Transf.* 50(9–10), 2007, 2002–18.

[49] Oztop HF, Abu-Nada E. Numerical study of natural convection in partially heated rectangular enclosures filled with nanofluids. *Int J Heat Fluid Flow.* 29(5), 2008, 1326–36.

[50] Brinkman HC. The viscosity of concentrated suspensions and solutions. *J Chem Phys.* 20(4), 1952, 571.

[51] Wasp EJ, Kenny JP, Gandhi RL. Solid--liquid flow: slurry pipeline transportation.[Pumps, valves, mechanical equipment, economics]. Ser Bulk Mater Handl; United States, 1(4), 1977.

[52] Maxwell JC. *A Treatise on electricity and magnetism*, second ed. Oxford Univ Press Cambridge. , 1904, 435–41.

[53] Hayat T, Nadeem S. Heat transfer enhancement with Ag–CuO/water hybrid nanofluid. *Results Phys.* 7, 2017, 2317–24.

[54] Khalili S, Dinarvand S, Hosseini R, Tamim H, Pop I. Unsteady MHD flow and heat transfer near stagnation point over a stretching/shrinking sheet in porous medium filled with a nanofluid. *Chinese Phys B.* 23(4), 2014, 48203.

[55] Suali M, Long N, Ishak A. Unsteady stagnation point flow and heat transfer over a stretching/shrinking sheet with prescribed surface heat flux. *Appl Math Comput Intell.* 1(1), 2012, 1–11.

[56] Wang CY. Stagnation flow towards a shrinking sheet. *Int J Non Linear Mech.* 43(5), 2008, 377–82.

[57] Bachok N, Ishak A, Pop I. The boundary layers of an unsteady stagnation-point flow in a nanofluid. *Int J Heat Mass Transf.* 55(23–24), 2012, 6499–505.

[58] Nayak AK, Singh RK, Kulkarni PP. Measurement of volumetric thermal expansion coefficient of various nanofluids. *Tech Phys Lett.* 36(8), 2010, 696–8.

[59] Kamyar A, Saidur R, Hasanuzzaman M. Application of computational fluid dynamics (CFD) for nanofluids. *Int J Heat Mass Transf.* 55(15–16), 2012, 4104–15.

ORCID iD

Saeed Dinarvand https://orcid.org/0000-0002-1625-8618

Mohammad Yousefi https://orcid.org/0000-0002-6785-3353

Ali. J. Chamkha https://orcid.org/0000-0002-8335-3121

Publisher's Note Shahid Chamran University of Ahvaz remains neutral with regard to jurisdictional claims in published maps and institutional affiliations.